

# Coherent backscattering of light off one-dimensional atomic strings

H. L. Sørensen, J.-B. Béguin, K. W. Kluge, I. Iakoupov, A. S. Sørensen, J. H. Müller, E. S. Polzik,<sup>\*</sup> and J. Appel<sup>\*</sup>  
*QUANTOP, Niels Bohr Institute, University of Copenhagen, Blegdamsvej 17, 2100 Copenhagen, Denmark*  
 (Dated: March 4, 2024)

We present the first experimental realization of coherent Bragg scattering off a one-dimensional (1D) system – two strings of atoms strongly coupled to a single photonic mode – realized by trapping atoms in the evanescent field of a tapered optical fiber (TOF), which also guides the probe light. We report nearly 12 % power reflection from strings containing only about one thousand cesium atoms, an enhancement of two orders of magnitude compared to reflection from randomly positioned atoms. This result paves the road towards collective strong coupling in 1D atom-photon systems. Our approach also allows for a straightforward fiber connection between several distant 1D atomic crystals.

PACS numbers: 78.47.jj, 37.10.Vz, 42.79.Dj

Keywords: nanofiber, Bragg reflection, waveguide, atoms, photonic crystal

In the search for systems suitable for quantum information technology, strong light-matter interaction achieved with guided photons has emerged as one of the favorites. Signatures of efficient coupling of guided photons have been reported for atoms [1] and quantum dots [2] coupled to photonic bandgap waveguides as well as for atoms in a hollow core fiber [3]. Atoms coupled to a TOF [4–6] offer strong coupling of photons to linear strings of about  $10^3$  atoms. This has been predicted to lead to long range interactions [7, 8] with prospects to simulate quantum many-body models [9] and the ability to generate arbitrary photonic number states [10, 11].

Bragg scattering, well known in crystallography, has become a powerful tool for artificial atomic structures such as optical lattices [12–17]. In free space, 1D optical lattices for atoms can be formed by interfering two beams and contain between hundreds and thousands of atoms in each disk-shaped trapping site. Here atoms are much stronger localized in the axial direction of the standing wave than in the two radial ones [16, 17]. Such systems have shown Bragg reflections of 5 % when probing hundreds of atomic planes [16] and 80 % when interacting with  $10^7$  atoms located in thousands of disks [17]. Similarly high reflection efficiencies have also been observed in periodically structured atomic ensembles in hot vapor cells [18].

In this letter, we combine the ideas of waveguiding and Bragg structuring. We show that with the tight confinement of a guided mode in a TOF just a thousand atoms are sufficient to create an efficient 1D mirror when arranged as linear strings fulfilling the Bragg condition.

The basic effect can be understood by considering each atom as a point scatterer. If the atomic ensemble is spatially unstructured, the phases of backscattered fields from individual atoms are uncorrelated. Waves emitted backwards thus add up incoherently and, for an optically thin sample, the total intensity is proportional to the number of scatterers. If, on the other hand, the atoms are arranged under the Bragg condition, spaced distances

$d = q\lambda_{\text{probe}}^{\text{TOF}}/2$  apart, where  $q$  is an integer and  $\lambda_{\text{probe}}^{\text{TOF}}$  is the wavelength of the probe light within the TOF [19], there is a fixed phase relation. This enhances the intensity by constructive interference and, in the limit of perfect arrangement, the reflected power scales quadratically with the number of scatterers for an optically thin medium.

In the experiment, we trap cesium atoms in a dual-color TOF-based lattice trap [4–6, 20] (details in SM.C), which holds the atoms as two 1D strings 200 nm above the surface on opposite sides of the fiber (see Fig. 1a,b). The distance between neighboring trap sites, which contain at most a single atom due to atomic collisions during the loading process [21], is set by the wavelength of the attracting standing wave trapping laser  $d_{\text{trap}} = \lambda_{\text{trap}}^{\text{TOF}}/2$ . To avoid trap-induced scattering,  $\lambda_{\text{trap}} = 1057$  nm is far-detuned from atomic resonance, whereas the probe light, at a vacuum wavelength  $\lambda_{\text{probe}} = 852$  nm, is near atomic resonance to ensure appreciable backscattering. The corresponding TOF wavelengths due to the fiber modal dispersion are  $\lambda_{\text{trap}}^{\text{TOF}} = 987$  nm and  $\lambda_{\text{probe}}^{\text{TOF}} = 745$  nm. With a sample length of  $\sim 1$  mm the incommensurate ratio  $\lambda_{\text{trap}}^{\text{TOF}}/\lambda_{\text{probe}}^{\text{TOF}}$  allows us to treat the atomic strings as originally completely unstructured with respect to the Bragg resonance, leading to a weak reflection as observed in [22].

Initially, all atoms are prepared in the same electronic ground state  $|\bullet\rangle \equiv (6^2S_{1/2}, F=4)$ . To turn the atomic strings into an effective Bragg mirror, the ensemble is structured with a short (250 ns) standing wave light pulse while the two-color TOF trap remains active. The frequency of the structuring light is detuned by  $-175$  MHz from the  $|\bullet\rangle \rightarrow (6^2P_{3/2}, F=3)$  transition to allow for propagation through the ensemble, which is opaque for resonant light (Fig. 1a and Fig. 1c).

The quasi-linearly vertically polarized structuring and probe fields possess vanishing longitudinal field components at the trapping sites, which ensures a high contrast of the structuring intensity grating experienced by the atoms. This choice of probe polarization leads to

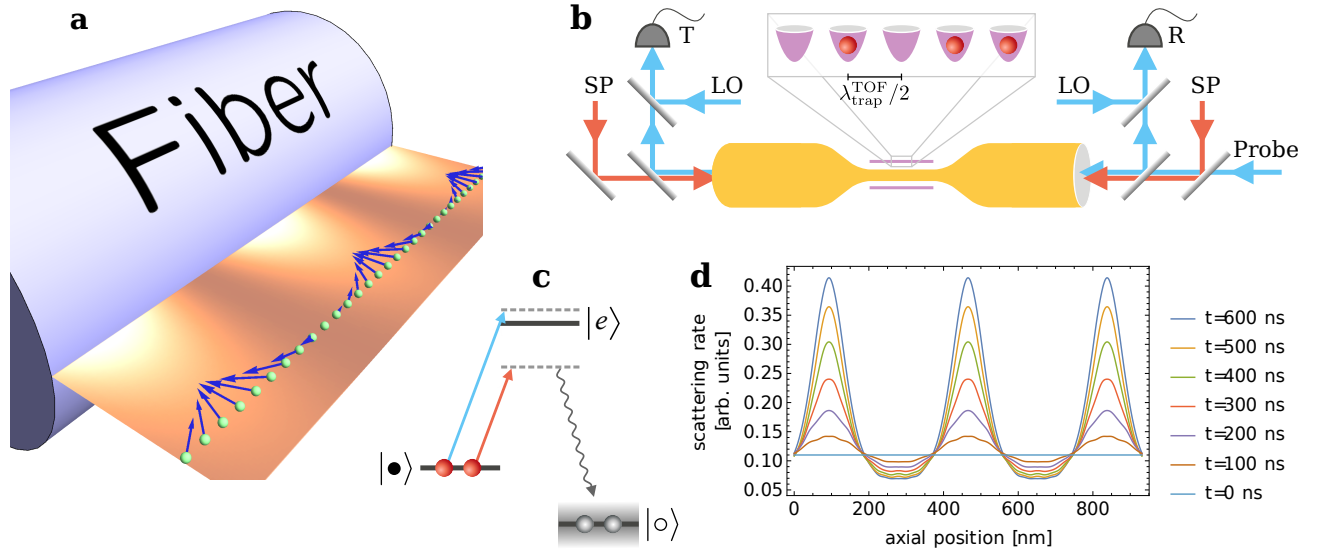


Figure 1. Experimental procedure and setup. **a**, The standing wave structuring pulse field (orange plane) accelerates atoms (green balls) both axially and radially towards the intensity maxima (bright spots). Since the trapping and structuring fields have incommensurate wavelengths, we depict with blue arrows the positions of atoms starting at the radial equilibrium location and various axial positions after a ballistic flight of 600 ns following the structuring pulse. **b**, Experimental setup. In the dipole trap, the atoms arrange themselves into two 1D strings (purple lines) along the TOF (yellow). Each trap site (purple wells in the zoom box) is either empty or contains a single atom prepared in the  $|\bullet\rangle$  state. A standing wave pulse (SP, red) is used to imprint a Bragg grating onto the atoms. A probe field (blue) is sent onto the atomic strings; the reflected and transmitted light is mixed with corresponding local oscillator (LO) beams and measured by two photo-detectors R and T (heterodyne detection). **c**, Level diagram. The probe beam (blue) is tuned close to resonance with the  $|\bullet\rangle \rightarrow |e\rangle \equiv (6^2P_{3/2}, F=5)$  transition. The structuring pulse (red) optically exerts both a radial and axial dipole force and pumps the atoms out of  $|\bullet\rangle$ . **d**, Evolution of the axial modulation of the scattering rate, calculated for an atomic ensemble located at the trap potential minimum (green balls in **a**) with an initial thermal velocity distribution corresponding to  $T = 42 \mu\text{K}$ .

an equal probability of scattered fields to couple into either the forward or backward TOF-guided mode, whereas for spin-preserving scatterers, the use of orthogonally polarized probe light would lead to predominant forward-scattering [23].

As the standing wave light pulse is sent through the TOF, it affects all atoms except the ones localized at its nodes. The coupling of the trapped atoms to the running wave probe field mode is changed by the structuring pulse through modulation of the atomic electronic and motional state (see Fig. 1d). Various physical effects, such as hyperfine pumping, Zeeman-level pumping, axial and radial acceleration due to dipole forces contribute to this modulation. We emphasize that the two-color TOF dipole trap is active during the entire structuring and Bragg scattering measurement sequence.

With the detuning and duration of the structuring light pulses chosen in this work, the effect of the dipole forces is dominant. For a structuring pulse tuned below the atomic resonance, atoms located distant to intensity nodes receive momentum radially towards the fiber and axially towards the closest antinode (see Fig. 1a). After a short time, this imprinted velocity grating transforms into a density- and coupling-modulation with maxima separated by multiples of half-wavelengths of the struc-

turing pulse, satisfying the Bragg condition in close analogy to a photo-refractive medium with a refractive index grating [24].

We measure the reflected and transmitted fields simultaneously by optical heterodyne detection (Fig. 1b) in an (adjustable) bandwidth of 9.2 MHz (details in SM.A) to avoid being affected by other stray light sources (such as the trap fields). As the effective mode area of the probe at the position of the atoms is small [25], we use an extremely weak probe field with a typical power of  $P_{\text{incident}} = 150 \text{ pW}$  to avoid saturation.

In Fig. 2, we present a typical example of the temporal dynamics of the reflectance (defined as the ratio of reflected to incident power  $P_{\text{reflected}}/P_{\text{incident}}$ ), for the structuring pulse present and absent. The curves are averaged over multiple consecutive experimental runs to overcome the shot noise due to the low photon flux in single experiments. With the incident probe power chosen well below saturation (see above), for every 60 input photons, on average only 4 photons impinge onto the reflection detector within the 96 ns sample time at the peak of the curve.

The probe is turned on at  $t = 0$  shortly after the structuring pulse has been turned off at  $t_0 = -0.3 \mu\text{s}$ . The peak power reflectance of  $(11.6 \pm 1.1) \%$  from the struc-

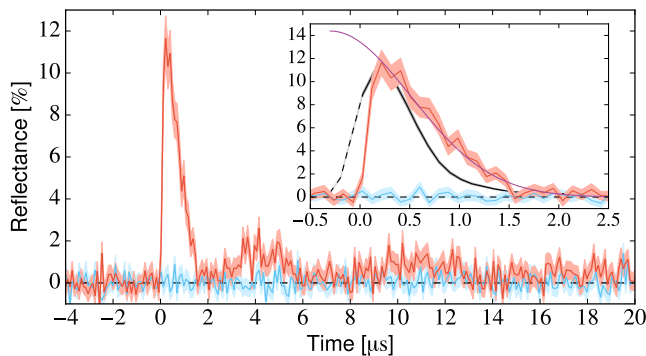


Figure 2. Reflectance off the atomic strings within a 2.8 MHz detection bandwidth (3 dB). The probe is tuned 8 MHz above atomic resonance and turned on at  $t = 0$  with an independently measured rise time of 80 ns. Blue curve: unstructured atomic ensemble, average of 250 experiments. Red curve: structured ensemble, average of 200 experiments. The shaded regions signify the one-sigma uncertainty interval with contributions from statistical averaging and a 5% input probe power fluctuation during the measurement. Inset: zoom on the first reflection peak with a fit to a Gaussian decay (purple) and the theoretical prediction (black) with uncertainty band given by the statistical averaging.

tured atoms, shown in Fig. 2, is two orders of magnitude stronger than the average reflectance of  $(0.10 \pm 0.01)\%$  observed from 1900 realizations of an unstructured ensemble.

As shown in the inset of Fig. 2, the decay after the maximum is well fitted by a Gaussian function  $f(t) = f(t_0) \exp[-(t - t_0)^2 / 2\tau^2]$  with a characteristic decay time  $\tau = (0.82 \pm 0.02) \mu\text{s}$ . We use the value of the fit function at  $t = 0.2 \mu\text{s}$  to extract robust values for the peak reflectance from the data. Physically, the reflectance depends on the degree of localization of atoms around the proper axial locations to fulfill the Bragg condition. The spatial ordering first builds up and then decays as atoms move past the focus points at the antinodes of the structuring wave pulse. In addition, any thermal random initial velocity on top of the deterministic imprinted velocity grating limits the quality of localization and accelerates the decay of ordering. After structuring, the atoms are left in a highly nonthermal motional state within the trap potential wells. We have verified that the weak probe laser itself does not influence the decay time of the reflectance signal (see SM.B).

Besides the significant reflection off the structured atoms following the probe onset, two much smaller peaks are visible after roughly  $4 \mu\text{s}$  and  $11 \mu\text{s}$  in Fig. 2. Reaching reflectances of  $(2.6 \pm 0.5)\%$  and  $(1.9 \pm 0.6)\%$  respectively, these signals are clearly distinguishable from a reflection off an unstructured ensemble. We attribute them to partial revivals of localization at the Bragg condition for the atomic wave packets sloshing and breathing in the incommensurate lattice of anharmonic trap wells.

For theoretical modeling, in separate measurements we determine the number of trapped atoms  $N_a$  for calibration purposes by counting the number of scattered photons required to optically pump all the atoms from  $|\bullet\rangle$  to  $(6^2S_{1/2}, F = 3)$  [6]. From the temporal dynamics of the pumping process, we can also extract the single-atom optical depth  $\alpha_0$ , albeit with a large relative uncertainty of about 25%, as such a measurement is affected by an unequal population distribution within the Zeeman sub-levels of  $|\bullet\rangle$  and broadening of the optical transitions due to the trapping fields. We obtain  $\alpha_0 = (0.51 \pm 0.13)\%$ , corresponding to an on-resonant saturation power of  $P_{\text{sat}} = \Gamma \hbar \omega / (2\alpha_0) = 750 \text{ pW}$  (i.e.  $\sim 100$  photons per excited state lifetime) for the  $|\bullet\rangle \rightarrow |e\rangle$ ,  $\Delta m_F = 0$  transition. The theoretical prediction for the overall reflectance is modeled by employing the 1D transfer matrix formalism [7, 15]: An initially random string of atoms is structured by spatially modulated dipole forces and hyperfine pumping. Its reflectance for probe light at any given time is evaluated by multiplying matrices describing the scattering off individual atoms alternating with matrices for free propagation (see SM.E for details). Inhomogeneous broadening of the probe transition by the strong trap light fields is taken into account by assigning a random Gaussian distributed detuning to each atom with a standard deviation of  $\sigma_\Delta = 0.41\Gamma$ , where  $\Gamma = 2\pi \times 5.23 \text{ MHz}$  denotes the natural linewidth of the atomic transition (see SM.F for details). The coupling of atoms to TOF-guided probe light at their radial equilibrium position is set to the experimentally determined value of  $\langle \alpha_0 \rangle = 0.51\%$  for the on-resonant optical depth per atom and scaled with the radial mode shape [26]. The initial radial position and velocity are randomized according to a thermal distribution with  $\langle T \rangle = 42 \mu\text{K}$ , about one fifth of the  $200 \mu\text{K}$  trap well depth. Radial motion due to the dipole force takes place in a harmonic oscillator potential with the independently measured radial trap frequency of  $85 \text{ kHz}$ , truncated at  $10 \text{ nm}$  from the TOF surface where atoms are irretrievably lost. For simplicity, dipole force induced axial motion is treated ballistically, which is justified since the observed dephasing times are much shorter than an axial oscillation cycle in the true trap potential ( $\omega_{\text{axial}} \simeq 100 \text{ kHz}$ ). In accordance with the experimental procedure, we average the simulation results over typically 100 random realizations.

In the inset in Fig. 2 the theoretical prediction for the reflection is shown to be in quantitative agreement with the peak reflectance. The faster temporal decay can be assigned to the simplified model not taking the true trap potential into account.

The observed critical dependence of reflectance on the degree of localization also strongly influences the conditions for achieving optimal reflectance. For a stronger structuring pulse the atomic wave packets become focused and localized faster, hence outrunning the dephasing by thermal motion. For a too strong structuring

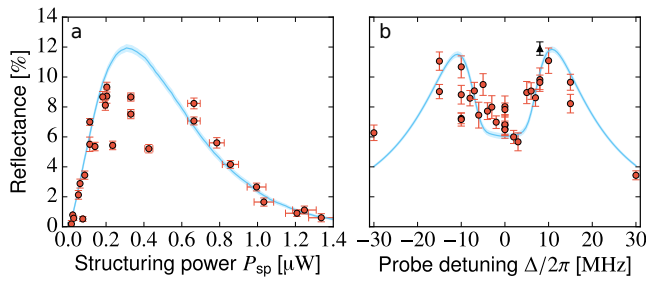


Figure 3. Experimental data. Each point represents the reflectance at  $t = 0.2 \mu\text{s}$  extracted from a Gaussian decay fit to 100–250 consecutive experimental runs with vertical error bars from the uncertainty on the fit parameters. Blue curves show the theoretical predictions with the shaded regions signifying the one-sigma uncertainty interval from the statistical averaging. **a**, Reflectance as a function of the power of the structuring pulse  $P_{\text{sp}}$  for a probe detuning of  $\Delta = 2\pi \times 8 \text{ MHz}$ . For this data  $\langle \tau \rangle = 0.89 \mu\text{s}$ . Horizontal error bars corresponds to a 5% power fluctuation. **b**, Variation of the reflectance with the probe detuning. The Bragg grating was created using a structuring power of  $0.2 \mu\text{W}$ . The black triangular point corresponds to the red data trace in Fig. 2. For this data  $\langle \tau \rangle = 0.86 \mu\text{s}$ .

pulse, however, the duration of high reflectivity decreases since a significant fraction of atoms climbs over the repulsive barrier of the trap and crashes into the hot fiber surface rapidly. This results in an optimal structuring pulse power due to the trade-off between a high degree of localization and a high number of remaining scatterers.

To visualize this trade-off, experimental data for the reflectance as a function of the structuring power  $P_{\text{sp}}$  is shown in Fig. 3a. Immediately before taking the data series,  $N_a$  was measured to be 1440. To confirm a stable initial atom number,  $N_a$  was measured again right after taking the data series to 1140. From this we assign  $N_a = 1290 \pm 150$ . Both the experiment and the model calculations, using the same input parameters for the simulation as above, show an optimum sample reflectance. The experimentally measured slopes on either side of the optimum are well captured by the model.

The influence of incomplete atomic localization is also evident when interrogating the atomic strings at varying detunings,  $\Delta = \omega_{\text{probe}} - \omega_a$ , of the probe laser from the atomic transition. If atoms were perfectly positioned, such as to fulfill the Bragg condition, the incident probe and backscattered fields would form a standing wave with nodes coinciding with the atom locations [16]. This reduces the absorption and allows the probe to propagate further into the sample, thereby increasing the number of scatterers contributing to the reflected field. In this case, the reflection spectrum is expected to be a Lorentzian with a maximum reflectance on resonance where the light-atom coupling is strongest [27]. When delocalized atoms are present, this description breaks down since diffuse scattering becomes prominent and increases the ab-

sorption. The penetration length of the probe thus becomes drastically reduced and the number of scatterers is effectively lowered. This can be circumvented by tuning the probe frequency slightly off-resonance and consequently decreasing the light-atom coupling [12, 16]. The detuned probe field then propagates further into the sample allowing for interaction with more atoms, which results in an increase in the coherent backscattering. In this regime, a reflection spectrum is expected to have a dip on resonance and maxima at probe detunings where the scattering probability is optimally balanced for high penetration depth. Experimental data confirming this is presented in Fig. 3b: The coherent Bragg reflection is the highest for detunings between 1.5 to 3 line widths from resonance. Using the same input parameters as above for the simulation we find satisfactory quantitative agreement between the data and the model.

In summary, we have shown that a truly one-dimensional dilute Bragg grating containing in total around a thousand atoms reflects more light than a solid slab of glass, reaching reflectances of more than 10%. The TOF trap platform offers exciting opportunities for future developments. The presented concept of creating a switchable Bragg-reflector by modulating the probe light coupling with standing-wave structuring light fields is versatile: instead of modifying the motional degrees of freedom of the atoms, optical pumping into other electronic states or coherent population transfer using a Raman process open paths to increase the lifetime of the reflection peak. Motional dephasing can be suppressed with colder atomic samples. The simulations predict that by applying the same structuring procedure at a temperature of  $T = 2 \mu\text{K}$  the reflectance can be doubled. Trapping the atoms permanently closer to the surface will increase the coupling and using a longer tapered fiber section will increase the overall atom number thus improving the reflectance. Adding an optical cavity with a modest finesse integrated with the fiber [28] will boost the single atom reflectivity to near unity. Such a cavity will reduce the present saturation photon number of about a hundred to the single photon level, thus allowing for strong single photon-light coupling in this 1D system. For these high coupling strengths, exploration and exploitation of atomic self-organization mechanisms [8] becomes an attractive playground for experiments. With these improvements the creation of resonantly structured atomic ensembles in the vicinity of photonic waveguides allows for new avenues in quantum state preparation [10] as well as for the formation of atomic cavities [7].

This work was supported by the ERC grants INTERFACE (grant no. ERC-2011-ADG 20110209) and QIOS (grant no. 306576), and the EU project SIQS (grant no. 600645). The authors would like to thank E. M. Bookjans for help in setting up the experiment.

*Note added* – During submission of our manuscript, we



became aware of a new related study [29].

---

\* Corresponding Authors: [polzik@nbi.dk](mailto:polzik@nbi.dk); [jappel@nbi.dk](mailto:jappel@nbi.dk)

- [1] A. Goban, C.-L. Hung, J. D. Hood, S.-P. Yu, J. A. Muniz, O. Painter, and H. J. Kimble, *Phys. Rev. Lett.* **115**, 063601 (2015).
- [2] P. Lodahl, S. Mahmoodian, and S. Stobbe, *Reviews of Modern Physics* **87**, 347 (2015).
- [3] M. Bajcsy, S. Hofferberth, V. Balic, T. Peyronel, M. Hafezi, A. S. Zibrov, V. Vuletic, and M. D. Lukin, *Physical Review Letters* **102**, 203902 (2009).
- [4] F. Le Kien, V. I. Balykin, and K. Hakuta, *Physical Review A* **70**, 063403 (2004).
- [5] E. Vetsch, D. Reitz, G. Sagué, R. Schmidt, S. T. Dawkins, and A. Rauschenbeutel, *Physical Review Letters* **104**, 203603 (2010).
- [6] J. B. Béguin, E. M. Bookjans, S. L. Christensen, H. L. Sørensen, J. H. Müller, E. S. Polzik, and J. Appel, *Physical Review Letters* **113**, 263603 (2014).
- [7] D. E. Chang, L. Jiang, A. V. Gorshkov, and H. J. Kimble, *New Journal of Physics* **14**, 063003 (2012).
- [8] D. E. Chang, J. I. Cirac, and H. J. Kimble, *Physical Review Letters* **110**, 113606 (2013).
- [9] J. S. Douglas, H. Habibian, C. L. Hung, A. V. Gorshkov, H. J. Kimble, and D. E. Chang, *Nature Photonics* **9**, 326 (2015).
- [10] A. González-Tudela, V. Paulisch, D. E. Chang, H. J. Kimble, and J. I. Cirac, *Phys. Rev. Lett.* **115**, 163603 (2015).
- [11] A. González-Tudela, V. Paulisch, H. J. Kimble, and J. I. Cirac, (2016), [arXiv:1603.01243](https://arxiv.org/abs/1603.01243).
- [12] G. Birkel, M. Gatzke, I. H. Deutsch, S. L. Rolston, and W. D. Phillips, *Physical Review Letters* **75**, 2823 (1995).
- [13] M. Weidemüller, A. Hemmerich, A. Görlitz, T. Esslinger, and T. W. Hänsch, *Physical Review Letters* **75**, 4583 (1995).
- [14] G. Raithel, G. Birkel, A. Kastberg, W. D. Phillips, and S. L. Rolston, *Physical Review Letters* **78**, 630 (1997).
- [15] I. H. Deutsch, R. J. C. Spreeuw, S. L. Rolston, and W. D. Phillips, *Physical Review A* **52**, 1394 (1995).
- [16] S. Slama, C. von Cube, M. Kohler, C. Zimmermann, and P. W. Courteille, *Physical Review A* **73**, 023424 (2006).
- [17] A. Schilke, C. Zimmermann, P. W. Courteille, and W. Guerin, *Physical Review Letters* **106**, 223903 (2011).
- [18] M. Bajcsy, A. S. Zibrov, and M. D. Lukin, *Nature* **426**, 638 (2003).
- [19] Throughout the paper  $\lambda$  with (without) the superscript “TOF” refers to the TOF (free-space) wavelength.
- [20] A. Goban, K. S. Choi, D. J. Alton, D. Ding, C. Lacroûte, M. Pototschnig, T. Thiele, N. P. Stern, and H. J. Kimble, *Physical Review Letters* **109**, 033603 (2012).
- [21] N. Schlosser, G. Reymond, and P. Grangier, *Physical Review Letters* **89**, 023005 (2002).
- [22] D. Reitz, C. Sayrin, B. Albrecht, I. Mazets, R. Mitsch, P. Schneeweiss, and A. Rauschenbeutel, *Physical Review A* **89**, 031804 (2014).
- [23] F. Le Kien and A. Rauschenbeutel, *Physical Review A* **90**, 023805 (2014).
- [24] The small relative wavelength difference between probe and structuring light  $\delta\lambda/\lambda = 5 \cdot 10^{-7}$  leads only to a negligible phase mismatch over the sample length ( $1 \text{ mm} \sim 10^3\lambda$ ).
- [25] F. Le Kien, V. I. Balykin, and K. Hakuta, *Physical Review A* **73**, 013819 (2006).
- [26] F. L. Kien, J. Q. Liang, K. Hakuta, and V. I. Balykin, *Optics Communications* **242**, 445 (2004).
- [27] F. Le Kien and A. Rauschenbeutel, *Physical Review A* **90**, 063816 (2014).
- [28] S. Kato and T. Aoki, *Physical Review Letters* **115**, 093603 (2015).
- [29] N. Corzo, B. Gouraud, A. Chandra, A. Goban, A. Sheremet, D. V. Kupriyanov, and J. Laurat, (2016), [arXiv:1604.03129](https://arxiv.org/abs/1604.03129).

## SUPPLEMENTARY MATERIAL

In the following, we provide additional information on experimental details and the numerical implementation of the theoretical model. In [SM.A](#), we provide technical details on our detection method. In [SM.B](#) we discuss influence by the probe on the temporal decay of the reflectance. The full experimental sequence is presented in [SM.C](#) followed by [SM.D](#) where additional experimental data for the sample transmittance is presented and discussed. The numerical procedure to obtain the theoretical predictions for the reflectance is specified in [SM.E](#), and finally, we conclude with [SM.F](#), in which we show how the amount of inhomogeneous broadening is estimated.

### SM.A: Detection

In the experiment, we measure the reflected and transmitted fields simultaneously by optical heterodyne detection (Fig. [1b](#)): Before entering the TOF, the probe is split from a strong ( $\approx 700 \mu\text{W}$  for the reflection detector) local oscillator (LO) reference beam and sent through an acousto-optical modulator to shift it in frequency by  $\Omega = 2\pi \times -62.5 \text{ MHz}$ . The transmitted and reflected fields are each superimposed with their corresponding LO using 90:10 beam splitters and detected with low-noise AC-photo-detectors. The recorded quadrature signals of the beat-note are digitally demodulated, low-pass filtered and converted into a photon flux, using independently both a calibrated power reference and the LO shot-noise level.

With a detection bandwidth of  $B_{3\text{dB}} = 0.89/t_{\text{sample}} = 9.2 \text{ MHz}$ , we determine the number of signal photons hitting the detector during the sample time  $t_{\text{sample}} = 96 \text{ ns}$  by

$$n_s = \frac{1}{\eta \mathcal{V}^2} \frac{\delta i_{\text{signal}}^2 - \delta i_{\text{sn+en}}^2}{\delta i_{\text{sn+en}}^2 - \delta i_{\text{en}}^2}, \quad (\text{A1})$$

where  $\eta = 0.89$  is the quantum efficiency of the detector,  $\mathcal{V} = 0.93$  is the measured interferometric visibility. The photocurrent signal  $s(t)$  is mixed down to base band and averaged over a time  $t_{\text{sample}}$  to obtain  $\delta i_{\text{signal}}^2(t) = \left| \int_t^{t+t_{\text{sample}}} e^{i\Omega t'} s(t') \frac{dt'}{t_{\text{sample}}} \right|^2$ . Its value with blocked probe input is  $\delta i_{\text{sn+en}}^2$ , and  $\delta i_{\text{en}}^2$  denotes the electronic noise of the detector as measured with both the probe- and the LO-beam blocked.

Including the amount of optical losses in the path from the atomic strings to the reflection detector of 54 %, we arrive at the number of photons reflected off the atoms.

### SM.B: Reflection lifetime

In Fig. [S1](#) we show the histogram of the fitted characteristic time constant  $\tau$  of the reflectance decay according to the Gaussian model function given in the main text.

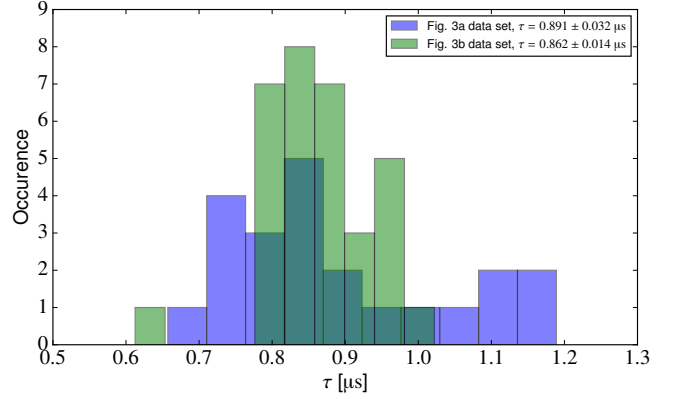


Figure S1. Histogram of  $\tau$  for the two data sets used in Fig. [3a,b](#). In the legend the mean value and the standard deviation of the mean of  $\tau$  is given.

To verify experimentally that the decay is not probe induced, we have performed a series of measurements with increasing delay between the end of the structuring pulse and the start of probe pulse as shown in Fig. [S2](#). If the

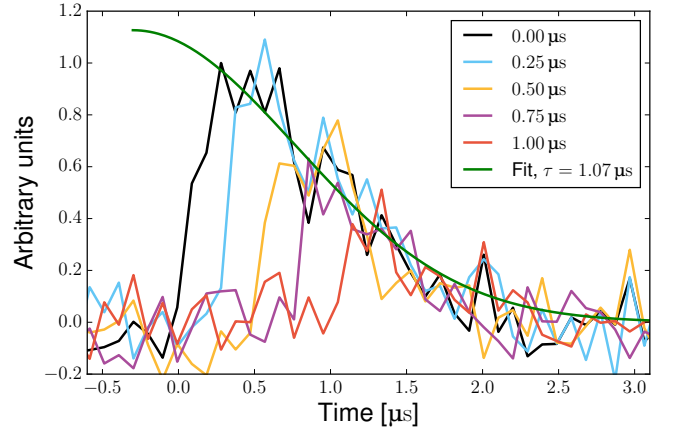


Figure S2. Result of the reflection measurements with delayed probe pulses. Error bars omitted for visual clarity. Each curve is an average over 100 consecutive experimental runs obtained for a 150 pW on-resonant probe.

reflectance lifetime were dominated by a destructive influence from the probe, we would expect to reach the same amount of reflection for the various time delays. This is clearly not the case. In Fig. [S2](#) we see that the decaying tails of the probe signals all follow the same global curve described by a single Gaussian decay fit to the black curve with probe onset at  $t = 0$ . We thus conclude that the probe itself does not have a significant

influence on the dephasing of the imprinted Bragg grating. We obtain the same results for greater probe powers and off-resonant probe light as well (not shown).

### SM.C: Experimental sequence

In each experiment, we first load cesium atoms from a background vapor into a standard 6-beam magneto-optical trap (MOT). This is followed by sub-Doppler cooling during which the atoms are loaded into a dual-color TOF-based trap [4–6, 20]; using two quasi-linearly horizontally polarized counter-propagating red-detuned fields with wavelength  $\lambda_{\text{trap}} = 1057$  nm and power  $P_{\text{trap}} \approx 2 \times 1.3$  mW together with a quasi-linearly vertically polarized blue-detuned field (with wavelength  $\lambda_{\text{blue}} = 780$  nm and power  $P_{\text{blue}} = 14$  mW) optical dipole traps are formed about 200 nm above the TOF surface, which hold the atoms as two 1D strings on both sides of the fiber (see Fig. 1a). After loading the atoms into this trap, the MOT beams are shut off and a waiting time of 11 ms is imposed to ensure that only trapped atoms are probed.

In Fig. S3 the timing for the different experimental steps for preparing and probing the single atomic Bragg grating is shown. The initial MOT loading and subsequent sub-Doppler cooling for transferring the atoms into the TOF trap takes  $\sim 2$  s. Prior to creating the Bragg grating an initial reference measurement for the fully transmitted field with beat note intensity  $I_0$  is established while having all the atoms in the transparent state  $|\circ\rangle$  (from  $t = -10$   $\mu\text{s}$  to  $t = -6$   $\mu\text{s}$ ) (see also Fig. S4). Immediately after, the atoms are optically pumped from

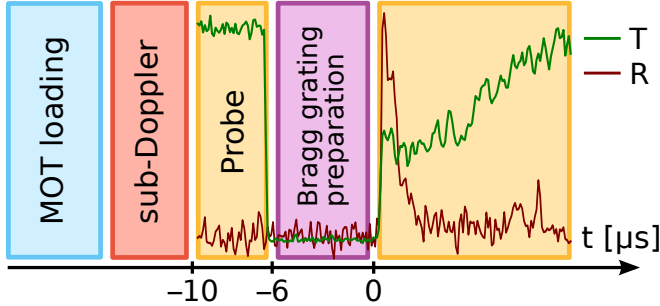


Figure S3. Time sequence of a single experimental run. Green (red) curve is an illustration of the transmitted (reflected) power (not to scale).

$|\circ\rangle$  to  $|\bullet\rangle$  in a duration of 3  $\mu\text{s}$ . This is followed by the structuring pulse creating the transient gradient of the light atom coupling. At  $t = 0$  the probe is turned back on. Measurements of both the reflected and transmitted fields are continuously carried out from  $t = -10$   $\mu\text{s}$  to  $t = 40$   $\mu\text{s}$ .

### SM.D: Transmittance

From the detected beat note intensity  $I_t$  of the transmitted light, the detuning dependent optical depth  $\alpha$  can be extracted via Lambert-Beer's law;  $\mathcal{T} = e^{-\alpha}$ , where

$$\mathcal{T} = \frac{I_t - I_{\text{bg}}}{I_0 - I_{\text{bg}}} \quad (\text{D1})$$

is the transmittance, see Fig. S4, and  $I_{\text{bg}}$  is the detection background when the probe is off from  $t = -6$   $\mu\text{s}$  to  $t = 0$  as shown in Fig. S3.

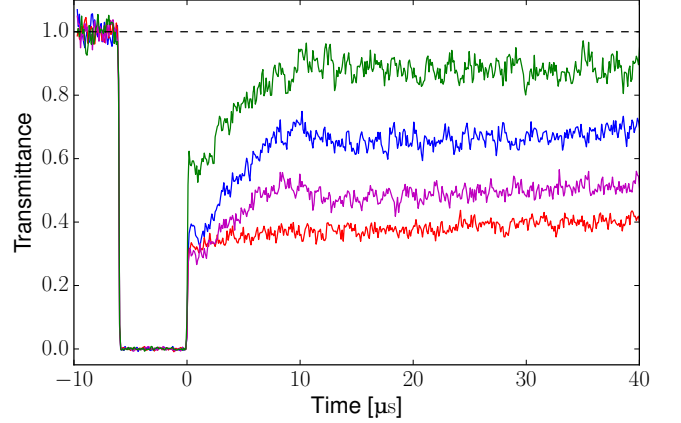


Figure S4. Transmittance. The traces are obtained for  $P_{\text{probe}} = 140$  pW,  $\Delta = 8$  MHz,  $N_a \approx 1300$ , and four different powers of the structuring pulse  $P_{\text{sp}}$ : Green:  $P_{\text{sp}} = 2 \times 1.0$   $\mu\text{W}$ , Blue:  $P_{\text{sp}} = 2 \times 0.2$   $\mu\text{W}$ , Purple:  $P_{\text{sp}} = 2 \times 0.09$   $\mu\text{W}$ , Red: no structuring.

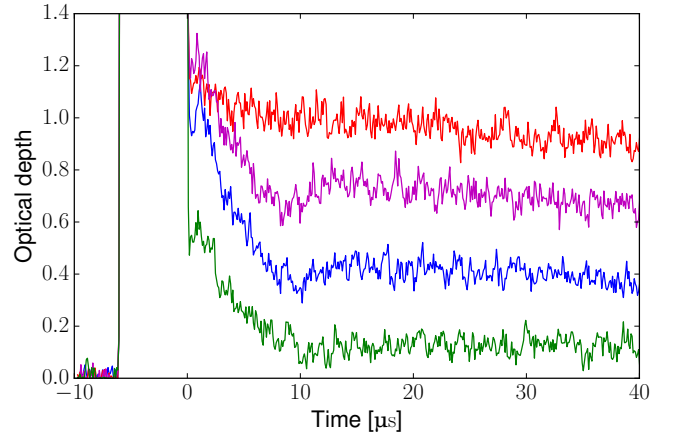


Figure S5. Extracted optical depth corresponding to the traces shown in Fig. S4.

In Fig. S5, we present the optical depth  $\alpha$  extracted from the corresponding transmittance shown in Fig. S4. The structured ensemble displays rich transmittance dynamics: During the life-time of the Bragg-reflection ( $t \approx 0 \dots 1$   $\mu\text{s}$ ) a rise in optical density is observed as the reflection decays. This is followed by a decrease of optical

depth, which is more pronounced for stronger structuring fields. Part of the initial rise stems from the decay of axial ordering leading to more scattering into free space modes. Another part of the initial rise can also be understood by the continuing inward radial motion of atoms increasing their coupling to the TOF guided modes. The subsequent decrease stems from fairly weak structuring fields mainly from atoms being reflected off the steep repulsive barrier and escaping towards the shallow part of the trap potential away from the fiber, where they are barely coupled before returning towards their start position after one oscillation cycle. Hints of oscillatory dynamics with a matching period of  $t = 12 \mu\text{s}$  can be seen in the blue and purple traces of Fig. S5. For stronger structuring fields a significant fraction of the atoms gains enough radial kinetic energy to climb over the repulsive barrier and collide with the fiber surface, at which point atoms cease to interact resonantly with the probe light. This leads to slightly faster and more pronounced loss of optical depth for strong structuring fields. In addition to radial kinetic energy the atoms also receive axial kinetic energy, which, together with the non-separability of the true trap potential, makes atoms with enough total energy never return to the vicinity of the fiber. The loss dynamics is essentially stationary after a little more than one radial oscillation cycle. We note that we observe quite similar dynamics in the simulation model, despite the simplified treatment of axial and radial motion, see Fig. S6. The final ( $t > 20 \mu\text{s}$ ) slow decrease of optical depth is also observed in the absence of structuring light and is due to the limited trap lifetime.

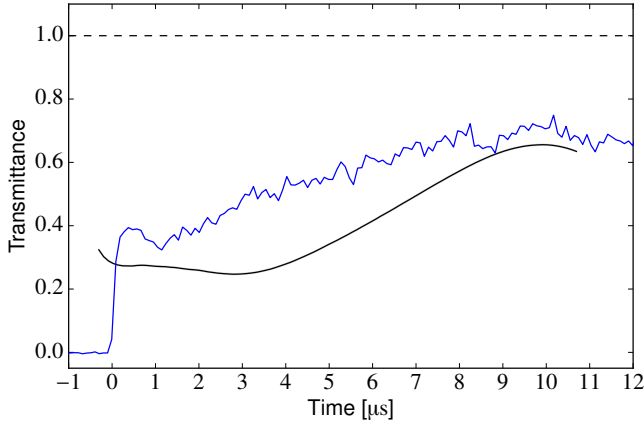


Figure S6. Zoom of blue transmittance curve in Fig. S4 together with the theoretical prediction (black).

### SM.E: Transfer matrix

For the theoretical modeling of the data presented here and in the main text we employ the transfer matrix for-

malism. Each atom is modeled as a two-level system in

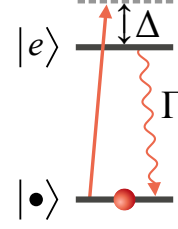


Figure S7. Two-level diagram.

the low saturation approximation characterized by a single scattering parameter

$$\beta_j = \frac{\Gamma_{1D}}{\Gamma' - 2i(\Delta + \Delta_j)}, \quad (\text{E1})$$

where the total radiative decay rate is given by  $\Gamma = \Gamma_{1D} + \Gamma'$  with  $\Gamma_{1D} = \alpha_0 \Gamma / 2$  and  $\Gamma'$  being the decay rates into the TOF mode and all other modes respectively,  $\Delta$  is the probe detuning from atomic resonance (Fig. S7), and  $\Delta_j$  is an additional shift that accounts for the inhomogeneous broadening of the atomic transition. Each  $\Delta_j$  is drawn from a Gaussian distribution with the width  $\sigma_\Delta$  (see the following section).

The transfer matrix for the  $j$ -th atom is

$$M_{a,j} = \begin{pmatrix} 1 - \beta_j & -\beta_j \\ \beta_j & 1 + \beta_j \end{pmatrix}. \quad (\text{E2})$$

If the position of the atom is  $z_j$ , then  $M_{a,j}$  relates  $E_R$  and  $E_L$  (right- and left-going electric fields respectively) at the position  $z_j^- = z_j - \epsilon$  (just to the left of the atom with an infinitesimal  $\epsilon$ ) to the fields at  $z_j^+ = z_j + \epsilon$  (just to the right of the atom). Writing this as an equation we have

$$\begin{pmatrix} E_R(z_j^+) \\ E_L(z_j^+) \end{pmatrix} = M_{a,j} \begin{pmatrix} E_R(z_j^-) \\ E_L(z_j^-) \end{pmatrix}. \quad (\text{E3})$$

The transfer matrices for free propagation between the atoms are

$$M_{f,j} = \begin{pmatrix} e^{ikd_j} & 0 \\ 0 & e^{-ikd_j} \end{pmatrix}, \quad (\text{E4})$$

where  $d_j$  is the propagation distance between atom  $j$  and atom  $j + 1$ , i.e.  $z_{j+1} = z_j + d_j$ . For the matrix  $M_{f,j}$ , it holds that

$$\begin{pmatrix} E_R(z_{j+1}^-) \\ E_L(z_{j+1}^-) \end{pmatrix} = M_{f,j} \begin{pmatrix} E_R(z_j^+) \\ E_L(z_j^+) \end{pmatrix}. \quad (\text{E5})$$

In the model, we neglect the effects of the axial trap potential and take the atoms to be initially uniformly distributed along the length of the ensemble. The procedure to obtain  $d_j$ 's is as follows:



- $N$  random numbers  $\{x_1, x_2, \dots, x_N\}$  are drawn from the uniform distribution on the interval  $[0, 1)$ .
- The positions of the atoms are given by  $z_j = Lx_j$ , where  $L$  is the total length of the ensemble.
- The distances between the atoms are then given by  $d_j = z_{j+1} - z_j$ , where we define  $z_{N+1} = L$ .

In addition, each atom is assigned a random axial thermal velocity drawn from a Gaussian distribution according to the temperature of the ensemble. Likewise, initial random radial positions and velocities are chosen.

To model the effect of hyperfine pumping, each atom is assigned a probability  $p_j$  to remain in the  $|\bullet\rangle$  state after the structuring pulse, with pumping strength quantified by the dimensionless parameter  $\zeta$ , given by

$$p_j = e^{-\zeta \cos^2(2\pi z_j / \lambda_{\text{sp}}^{\text{TOF}})}, \quad (\text{E6})$$

for the case of atoms not saturated by the structuring light. The probability for being pumped from  $|\bullet\rangle$  to  $|\circ\rangle$  is thus  $1 - p_j$ . In the numerical implementation, this is taken into account by drawing  $N$  random numbers from a uniform distribution on  $[0, 1)$  and comparing them with  $p_j$  for each atom. The probability of such a random number to be smaller than  $p_j$  is equal to  $p_j$  and the probability to be bigger than  $p_j$  is equal to  $1 - p_j$ . The advantage of this approach is that once the array of the random numbers is fixed, the depumping process becomes deterministic in this model for any choice of the pumping strength  $\zeta$ . For the depumped atoms,  $M_{a,j}$  is replaced by the identity matrix. We remark that for the short duration and range of intensities of the structuring pulses chosen in the experiment the amount of hyperfine pumping is quite limited, e.g. at pulse parameters for highest reflectance less than 10 % of the atoms are pumped into the  $|\circ\rangle$  level. It is, nevertheless, important to take the effect into account for good quantitative agreement between model and experiment.

The effect of dipole forces in axial and radial directions is modelled by evaluating for each atom the received momentum kick according to position in the structuring pulse standing wave with the given duration, detuning and intensity. Isotropic distribution over Zeeman levels is assumed and all excited hyperfine levels of the atomic transition are taken into account. Position and velocity at the instant of probing is then determined applying the propagators for ballistic (harmonic) motion in the axial (radial) direction. Each atom receives updated  $\Gamma_{1D}$  and  $\Gamma'$  values for the current radial distance to the fiber according to the shape of the evanescent guided modes. For an atom  $j$ , which has come closer to the fiber than a cut-off radius of 10 nm at any time between structuring and the instant of probing, the transfer matrix  $M_{a,j}$  is replaced by the identity matrix.

The theoretical curves in the main text are obtained by

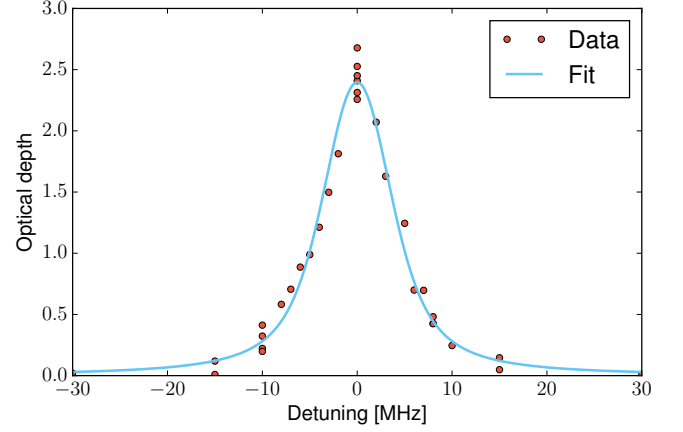


Figure S8. Optical depth as a function of the probe detuning. Data points are derived from the transmission signals for the reflectance data presented in Fig. 3b in the main text.

averaging over typically 100 realizations in the following way:

- For each realization the transfer matrix for the ensemble is found

$$M_{\text{ensemble}} = M_{f,N} M_{a,N} \dots M_{f,1} M_{a,1}. \quad (\text{E7})$$

- If  $M_{\text{ensemble}}$  is written out as

$$M_{\text{ensemble}} = \begin{pmatrix} M_{11} & M_{12} \\ M_{21} & M_{22} \end{pmatrix}, \quad (\text{E8})$$

then the (amplitude) reflection coefficient for the whole ensemble is given by  $r = M_{12}/M_{22}$ . The (amplitude) transmission coefficient is  $t = 1/M_{22}$ .

- As the final step, we take the mean of the absolute square of the reflection (transmission) coefficient  $|r|^2$  ( $|t|^2$ ) to obtain the reflectance (transmittance).

Averaging over many ensemble realizations still gives stochastic results, but the standard deviation of the mean reflection and transmission coefficients can be decreased by using a larger number of ensemble realizations and hence can be made arbitrarily small.

### SM.F: Inhomogeneous broadening

To estimate the amount of inhomogeneous broadening of the atomic transition, we fit the inferred optical depth as a function of the probe detuning (Fig. S8) with a Voigt profile:

$$V(\Delta; \sigma_\Delta, \alpha) = \int_{-\infty}^{\infty} G(\Delta', \sigma_\Delta) L(\Delta - \Delta') d\Delta'. \quad (\text{F1})$$

Here  $G$  and  $L$  are the Gauss- and Lorentz-distributions given by:

$$G(\Delta', \sigma_\Delta) = \frac{1}{\sqrt{2\pi}\sigma_\Delta} \exp\left(-\frac{\Delta'^2}{2\sigma_\Delta^2}\right), \quad (\text{F2})$$

$$L(\Delta - \Delta') = \frac{\alpha}{1 + (\Delta - \Delta')^2/(\Gamma/2)^2 + s}. \quad (\text{F3})$$

$s = P/P_{\text{sat}} = 150 \text{ pW}/750 \text{ pW} = 0.2$  is the saturation parameter. The free parameters in the fit are the homogeneous on-resonant optical depth  $\alpha$ , and the inhomogeneous broadening  $\sigma_\Delta$ .